Microbial Engineering of Nanoheterostructures: Biological Synthesis of a Magnetically Recoverable Palladium Nanocatalyst

Victoria S. Coker,[†,*] James A. Bennett,[‡] Neil D. Telling,[†,§] Torsten Henkel,[†] John M. Charnock,[†] Gerrit van der Laan,[†,⊥] Richard A. D. Pattrick,[†] Carolyn I. Pearce,[†,∥] Richard S. Cutting,[†] Ian J. Shannon,[‡] Joe Wood,[¶] Elke Arenholz,[#] Ian C. Lyon,[†] and Jonathan R. Lloyd[†]

[†]School of Earth, Atmospheric & Environmental Sciences and Williamson Research Centre for Molecular Environmental Science, University of Manchester, Manchester M13 9PL, U.K., [‡]School of Chemistry, University of Birmingham, Birmingham B15 2TT, U.K., [§]Institute for Science and Technology in Medicine, Keele University, Stoke-on-Trent ST4 7QB, U.K., [⊥]Diamond Light Source Ltd., Didcot, Oxfordshire OX11 0DE, U.K., [∥]Chemical and Materials Sciences Division, Pacific Northwest National Laboratory, Richland, Washington 99352, [¶]School of Chemical Engineering, University of Birmingham, Birmingham B15 2TT, U.K., and [#]Advanced Light Source, Lawrence Berkeley National Laboratory, Berkeley, California 94720

ABSTRACT Precious metals supported on ferrimagnetic particles have a diverse range of uses in catalysis. However, fabrication using synthetic methods results in potentially high environmental and economic costs. Here we show a novel biotechnological route for the synthesis of a heterogeneous catalyst consisting of reactive palladium nanoparticles arrayed on a nanoscale biomagnetite support. The magnetic support was synthesized at ambient temperature by the Fe(III)-reducing bacterium, *Geobacter sulfurreducens*, and facilitated ease of recovery of the catalyst with superior performance due to reduced agglomeration (*versus* conventional colloidal Pd nanoparticles). Surface arrays of palladium nanoparticles were deposited on the nanomagnetite using a simple one-step method without the need to modify the biomineral surface, most likely due to an organic coating priming the surface for Pd adsorption, which was produced by the bacterial culture during the formation of the nanoparticles. A combination of EXAFS and XPS showed the Pd nanoparticles on the magnetite to be predominantly metallic in nature. The Pd^0—biomagnetite was tested for catalytic activity in the Heck reaction coupling iodobenzene to ethyl acrylate or styrene. Rates of reaction were equal to or superior to those obtained with an equimolar amount of a commercial colloidal palladium catalyst, and near complete conversion to ethyl cinnamate or stilbene was achieved within 90 and 180 min, respectively.

KEYWORDS: palladium · magnetite · Fe(III)-reducing bacteria · catalysis · Heck reaction · nanoparticle

Nanoparticles make highly desirable catalysts, often offering unique properties linked to their very high surface area. Palladium placed on a suitable support material makes an exceptional catalyst well-known for mild reaction conditions and exhibiting excellent compatibility with many polar functional groups and a high degree of chemo-, regio-, and even stereoselectivity.[1] Magnetic nanoparticles are particularly useful support materials for catalysts as they can combine the advantages of high dispersion through a liquid with ease of recovery.[2−6] Thus, coating magnetic nanoparticles with precious metals such as palladium results in a highly functional catalyst.[7−11] Conventional chemical approaches to make these materials have achieved varying degrees of success, as loss of precious metal during recycling can be a problem, and complicated protocols are often employed to functionalize the support material surface.[3,7,9,12−14]

On the basis of earlier work,[15] recent studies have revealed that biosynthetic routes can be harnessed to make nanoparticles of magnetite (Fe_3O_4) efficiently and at low cost with control over the magnetic properties by substitution of transition metals into the spinel ferrite structure.[16−18] Two routes are possible for the biological synthesis of nanoscale magnetite. In the first, magnetotactic bacteria synthesize intracellular crystals of single domain magnetite. These are used by the bacteria to orientate the cell within the Earth's magnetic field, helping the organism to guide itself to the sediment−water interface, its preferred ecological niche.[19,20] However, for this route, growth yields and, indeed, final yields of intracellular magnetite are very low. In the second route, dissimilatory Fe(III)-reducing bacteria such as *Geobacter* species can produce copious quantities of extracellular nanoscale magnetite through the respiration of poorly crystalline Fe(III) oxides and oxyhydroxides.[15] These specialist anaerobic bacteria live in environments depleted of oxygen and therefore conserve

*Address correspondence to vicky.coker@manchester.ac.uk.

Received for review December 9, 2009 and accepted March 31, 2010.

Published online April 15, 2010.
10.1021/nn9017944

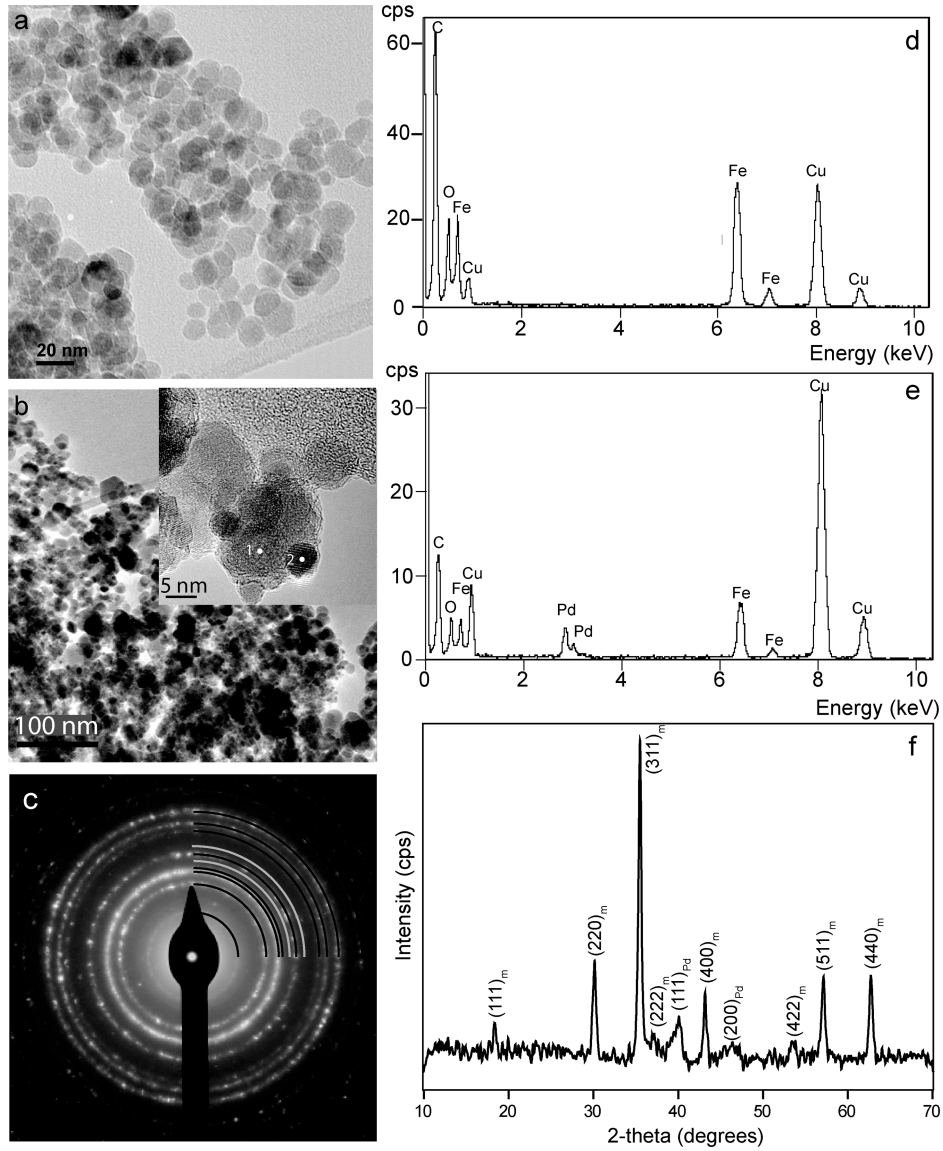

Figure 1. TEM images of (a) biomagnetite and (b) Pd-coated biomagnetite; inset contains annotation indicating where EDX spectra were taken. (c) Selected area electron diffraction (SAED) pattern for Pd-coated biomagnetite with reflections labeled in black (magnetite) and gray (palladium); (d) energy-dispersive spectra (EDS) of point 1 on image b; (e) EDS of point 2 on image b; (f) X-ray diffraction (XRD) of Pd-coated biomagnetite.

energy for growth by transferring electrons from the oxidation of simple carbon sources, such as acetate, to Fe(III) or Mn(IV)-bearing minerals.[21] This mechanism of nanomagnetite formation involves the extracellular reduction of Fe(III)−oxyhydroxides causing the release of soluble Fe(II), resulting in complete recrystallization of the amorphous mineral into the new, relatively reduced, highly crystalline magnetic phase.[22,23] Especially relevant to manufacturing, these enzyme-driven reactions take place on the scale of hours, at ambient pressures and temperatures and use inexpensive feedstocks.[22] Thus, nanoscale biomagnetite is a potential support material for industrial catalysts, especially if simplified protocols for functionalizing the bionanomineral surface can be developed.

Here we describe the bioproduction of such a catalyst comprising biomagnetite functionalized with palladium nanoparticles and involving a minimal level of processing. The effectiveness of this catalyst is demonstrated for the Heck coupling of iodobenzene with styrene or ethyl acrylate. Heck chemistry is of wide-ranging industrial importance, providing a single-step route to the arylation, alkylation, or vinylation of various alkenes.[24,25] Traditionally, a palladium−phosphine catalyst is used, although a large amount of literature is devoted to the study of a variety of different catalysts for these reactions.[24,26] This work opens the door to the development of an energy-efficient, environmentally friendly route to manufacture novel magnetic heterostructures which can be employed in a wide range of applications.

RESULTS AND DISCUSSION

A biogenic nanoscale magnetite support was first produced by anoxic washed cell suspensions of *Geobacter sulfurreducens* challenged with Fe(III)−oxyhydroxide, an electron donor (sodium acetate), and a redox mediator [9,10-anthraquinone-2,6-disulfonate (AQDS)]. After approximately 8 h, the Fe(III)−oxyhydroxide had been completely converted to magnetite. Production of the functionalized Pd-coated magnetite was concluded through the addition of a solution of $NaPdCl_4$ to the water-washed nanomagnetite suspension under an anoxic atmosphere (N_2/H_2 = 97:3); optimization studies revealed that removal of soluble palladium occurred rapidly, within an hour, and was efficient over a range of Pd(II) concentrations up to 10 mol % of Pd.

Detailed examination was undertaken of a nanomagnetite functionalized with a ~5 mol % Pd loading, produced by mixing the Pd(II) solution and biomagnetite for 12 h prior to washing in deionized water. Transmission electron microscope (TEM) images of the material produced before (Figure 1a) and after (Figure 1b) precipitation of Pd onto the surface of biomagnetite are shown. Figure 1a shows the magnetite to have a consistent particle size range of 20 to 30 nm. However, after addition of Pd, two sizes of particle became clearly visible; the high-resolution inset in Figure 1b shows how smaller particles (~5 nm) are attached to the larger particles (~20 nm). Energy-dispersive X-ray (EDX) analysis using a relatively unfocused beam showed the bulk sample (Figure 1b) to contain ~3.5 atom % Pd. Using an EDX spot size of 5−6 nm, analyses (Figure 1b inset, point 1; Figure 1d) indicated that the larger particles contained less than 1 atom % Pd, whereas analyses centered on the smaller particles (Figure 1b inset, point 2; Figure 1e) suggested that they were enriched for the precious metal (9−10 atom % Pd). These results indicate that the larger particles are the biomagnetite crystals decorated with small Pd particles. Both small and large particles displayed continuous lattice fringes, indicative of crystalline single crystals. TEM selected area electron diffraction (SAED) analysis (Figure 1c) of the particles with supporting data from powder X-ray diffraction (PXRD) (Figure 1f) confirmed that the material contained Bragg reflections, consistent with the presence of magnetite with less pronounced reflections consistent with Pd metal; the latter are broader than those for magnetite owing to their smaller particle size. Crystallite size was estimated by applying the Scherrer equation to the (311) peak of magnetite in Figure 1f, which resulted in a mean crystallite size of 27.2 nm, consistent with the size estimate from electron microscopy imaging. In addition, although much weaker, it was possible to obtain an estimate of the Pd crystallite size from the Pd (311) peak, which gave a value of ~5 nm, again in good agreement with TEM images.

In most examples of supported Pd catalyst manufacture, an organic ligand or silica shell is used to aid attachment of the Pd to the support,[8,9] for example, 3-aminopropyl triethoxysilane (APTS).[8] However, in the case of biogenic magnetite, no precoating with a ligand was required. Thus, to characterize the surface of biogenic magnetite, samples prior to Pd(II) addition were analyzed using time-of-flight secondary ion mass spectrometry (TOF-SIMS), as this technique is very sensitive to both organic and inorganic compounds. Images of different secondary ions (SI) associated with either Fe, Al, or organic material on the surface of a washed biogenic nanomagnetite (Figure 2a) were compared to the maps from a synthetically produced nanomagnetite (Alfa Aesar, Heysham, UK) (Figure 2b). Figure 2 illustrates that there is a significant quantity of organic material associated with the biogenic magnetite, as the representative secondary ion images of organic molecules spatially correlate with the Fe map, whereas the inorganic magnetite showed no significant organic signature corresponding to the spatial distribution of Fe. Depth profiling of the organic layer using C_{60} primary ions (PI) indicated that the organic layer is indeed a coating on the nanomagnetite. One bombardment of ~10^{15} PI/cm^2 resulted in a decrease of the SI signals associated with the organic material by a factor of approximately 100 (Figure 2c), whereas the SI signals associated with the nanomagnetite stayed almost constant.

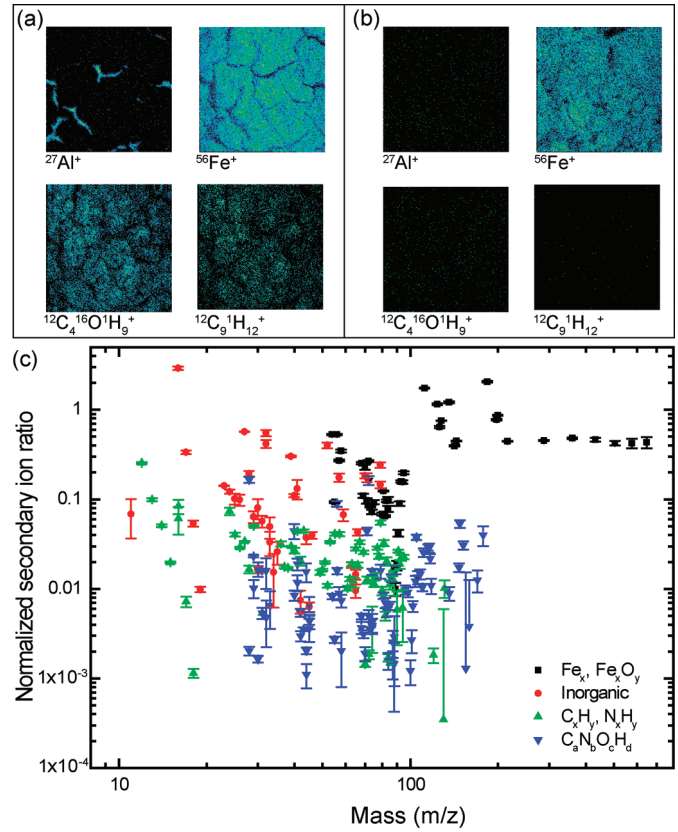

Figure 2. TOF-SIMS images of (a) washed biogenic nanomagnetite produced by *Geobacter sulfurreducens* and (b) commercially available inorganic nanomagnetite. Normalized secondary ion ratio of the surface of washed biogenic magnetite before and after ablation of the surface with a C_{60} gun.

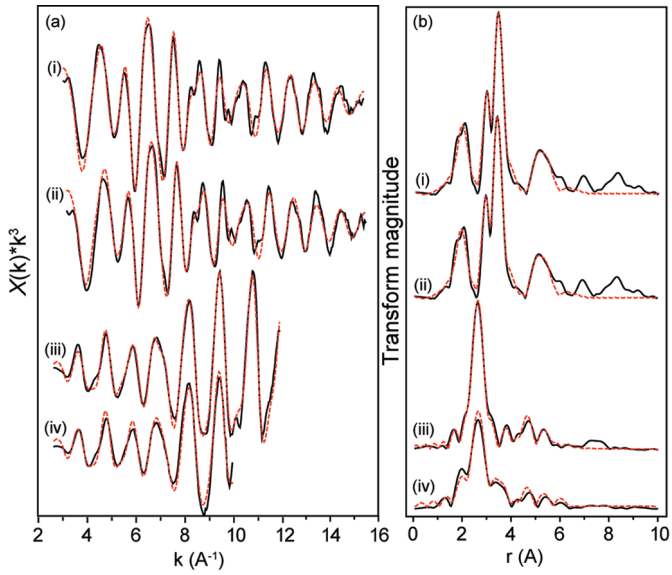

Figure 3. (a) EXAFS and (b) corresponding Fourier transform for the Fe *K*-edge of (i) biomagnetite and (ii) Pd-coated biomagnetite and Pd *K*-edge of (iii) Pd foil and (iv) Pd-coated biomagnetite. Data (black lines) and fits (dotted red lines).

Some of the secondary ion ratios for the Fe-bearing clusters in Figure 2c are below a value of 1, as ionization efficiencies change slightly with decreasing amounts of organic material. The presence of an organic coating explains the ability of the nanomagnetite to adsorb Pd without the need to precoat the washed nanoparticles prior to introducing the Pd solution. A likely source of the organic material is the extracellular polymeric substance (EPS), commonly produced by bacterial pure cultures and communities, and found previously bound to biogenic uranium nanoparticulate material.[27] We are not, however, excluding the presence of other cell exudates or constituents released after lysis of dead cells.

Using X-ray absorption (XA) spectroscopy, the Fe *K*-edge absorption spectra of biomagnetite before and after the addition of Pd were collected to provide the extended X-ray absorption fine structure (EXAFS) (Figure 3a (i,ii) and Table 1) and their corresponding Fourier transform (Figure 3b (i,ii) and Table 1). The EXAFS data provided an excellent fit for a magnetite structure for both samples, with the bond lengths for the tetrahedral (T_d) and octahedral (O_h) sites showing slight shortening after addition of Pd from 1.85 to 1.80 Å and from 2.03 to 2.00 Å, respectively. Incorporating Pd atoms did not improve the fit, indicating that the nanoparticulate Pd attached directly to the iron cations in magnetite or *via* bridging oxygens, however this was below the limit of detection. XA was additionally used to obtain the Fe $L_{2,3}$-edge in oppositely oriented magnetic field and thus provide the X-ray magnetic circular dichroism (XMCD) difference spectra of these samples (Figure 4a). The Fe $L_{2,3}$-edge XMCD can distinguish between the three Fe cation environments present in ferrite spinel structures to a depth of ~65 Å as the intensities of the peaks labeled in Figure 4a (i) relate to the amount of Fe^{2+} O_h (octahedral), Fe^{3+} T_d (tetrahedral), and Fe^{3+} O_h, respectively (see refs 28−30 for details). Figure 4a (i) displays the Fe $L_{2,3}$-edge XMCD spectrum for biomagnetite without addition of Pd that after fitting gave an Fe^{2+}/Fe^{3+} ratio of 0.64, indicating an excess of Fe^{2+} compared to a typical stoichiometric magnetite which would have a ratio of 0.50, consistent with previous results for biogenic magnetites.[31,32] The addition of Pd resulted in an increase in the amount of Fe^{2+}, forming a spinel with an Fe^{2+}/Fe^{3+} ratio of 0.70 (Figure 3b). The reduction of Fe^{3+} to Fe^{2+} in the spinel relates, most likely, to the ability of Pd^0 nanoparticles to absorb large quantities of hydrogen, which then interacts with the outer Fe atoms causing reduction to Fe^{2+}.

TABLE 1. Parameters Obtained from Fitting the Fe and Pd *K*-Edges EXAFS Spectra of Biomagnetite Samples[a]

	atom type	*N*	*r* (Å)	$2\sigma^2$ (Å^2)
		Fe *K*-edge		
biomagnetite	O	1.3	1.85	0.039
	O	4	2.03	0.025
	Fe	4	3.00	0.021
	Fe	8	3.50	0.012
	O	4	3.36	0.027
Pd biomagnetite	O	1.3	1.80	0.037
	O	4	2.00	0.024
	Fe	4	2.99	0.024
	Fe	8	3.48	0.012
	O	4	3.28	0.009
		Pd *K*-edge		
Pd foil standard	Pd	12	2.74	0.012
	Pd	6	3.85	0.020
	Pd	24	4.77	0.020
	Pd	12	5.36	0.012
	Pd	24	6.14	0.029
Pd biomagnetite	Pd	12	2.74	0.014
	Pd	6	3.84	0.018
	Pd	24	4.79	0.030
	Pd	12	5.42	0.016
	Pd	24	6.08	0.030

[a] *N* is the coordination number, *r* is the interatomic distance, and $2\sigma^2$ is the Debye−Waller factor.

EXAFS and X-ray photoelectron spectroscopy (XPS) were used to determine the nature of the Pd particles deposited on the surface of the magnetite. EXAFS and the related Fourier transform from the Pd *K*-edge (Figure 3a,b (iv)) for Pd−biomagnetite could be fitted with five coordination shells of atoms with the first shell containing 12 Pd scatterers at 2.74 Å and the second shell containing 6 Pd scatterers at 3.84 Å (see Table 1); these data have an excellent correspondence to values for Pd metal foil (Figure 3a,b (iii) and Table 1). Fitting the Pd 3d XPS spectrum (Figure 4b) indicated that the main Pd peak had a binding energy of 335.3 eV with a minor peak (6% intensity) at a binding energy of 336.8 eV. These compare well with literature values that show the main peak to be Pd^0,[33] and the weak peak to be a

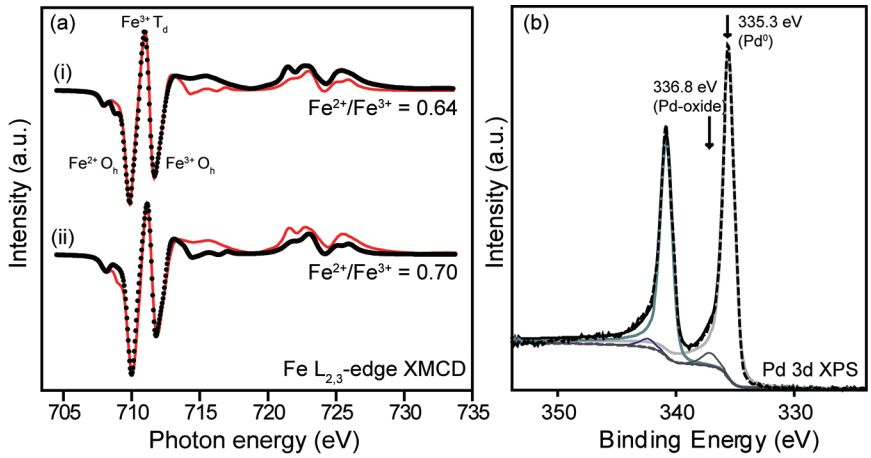

Figure 4. (a) Fe $L_{2,3}$-edge XMCD spectra of (i) biomagnetite and (ii) Pd-coated biomagnetite and (b) XPS of the Pd 3d peaks of biogenic Pd-coated magnetite.

second phase that may be PdO or PdO_2.[34] Pd−oxide could be present due to either oxidation of the surface of the metallic Pd or the Pd nanoparticles could be attaching to the magnetite *via* "bridging" oxygens. Additional XPS data (not shown) indicated that the surface of the nanoparticles had an Fe/Pd ratio of 1.00:0.22. Thus, the TEM, XAS, and XPS data are consistent and confirm the presence of Pd^0 nanoparticles attached to a biomagnetite support. Samples were kept under anoxic conditions throughout the preparation and measurement when using the surface-sensitive techniques XMCD and XPS to ensure that the samples were not oxidized by exposure to air.

The definitive test of the usefulness of the 5 mol % Pd-coated biomagnetite is its catalytic potential, and therefore, Heck reaction coupling of iodobenzene to styrene or ethyl acrylate was performed. Identical catalytic testing was also carried out on colloid-stabilized nanoparticulate palladium[35−37] as a means of comparing the Pd-coated biomagnetite to a highly active conventional catalyst. The Pd-coated biomagnetite was found to be active in the coupling of both olefins, with the complete conversion of the iodobenzene (plus ethyl acrylate or styrene) to ethyl cinnamate or stilbene within 90 and 180 min, respectively. Rates of reaction were equal or superior to those obtained with an equimolar amount of Pd from the colloidal palladium catalyst. However, the advantage of the magnetite-based catalyst was that it could be readily recovered at the end of the reaction by simply decanting the solution from the reaction vessel while retaining the solid catalyst by applying a magnetic field to the base of the flask. The solid was washed and dried before use in subsequent reactions.

Successive runs were performed for the Heck coupling of iodobenzene and ethyl acrylate to test the Pd-coated magnetite for recyclability. Although a small decrease in initial reaction rate was observed in each successive cycle, virtually quantitative conversions were reached in 120 min for each run, up to a fourth cycle (Figure 5), an improvement on some literature values for conventional catalysts.[8] These experiments were conducted without attempting to exclude air, and the decrease in activity is attributed to the loss of a small amount of material due to oxidation of some of the magnetite support to a nonmagnetic phase material, which was not recovered between runs, rather than direct loss of Pd to solution. Indeed, ICP-AES analysis of the supernatant in each cycle confirmed that there was negligible loss of Pd or indeed Fe to solution (data not shown). By comparison, although the palladium colloids remained catalytically active for a second cycle of the ethyl acrylate coupling, the halide conversion was only 89% compared to >99% for Pd-coated biomagnetite (Figure 5). In addition, more than 75% of the mass of the catalyst was lost during the recovery step, most likely due to the tertiary butyl ammonium bromide capping layer dissolving in the solvent. This would lead to the remaining palladium aggregating, reducing the active surface area substantially. Further recycling after the second run was unfeasible due to the very low mass of remaining material.

These results demonstrate that a novel biomagnetite-supported Pd nanoparticle catalyst has several major advantages over conventional colloidal

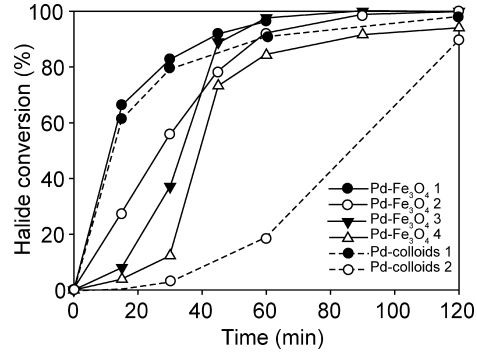

Figure 5. Rate of conversion during the Heck coupling of iodobenzene and ethyl acrylate catalyzed by Pd-coated biomagnetite (solid lines) or Pd colloids (dashed lines). Fresh catalyst was used in run 1, and runs 2−4 used recycled catalyst.

Pd catalysts. First, recovery and recycling is facile, and second, the biomagnetite support keeps the Pd dispersed and prevents it from agglomerating and losing vital surface area. The preparation method, apart from its novelty, provides an organics-coated ferrite particle in a one-step process, allowing Pd nanoparticles to be attached to the support material without further processing. Bacterial production is a low-cost, environmentally friendly biotechnological route of manufacture, which opens up a route to the manufacture of other precious metal nanocatalysts. Recent success at applying gold- and platinum-derived materials to biogenic magnetite as supported nanoparticles (unpublished data) indicates the versatility of bacterial production of nanocatalysts, which could be applied to a wide range of catalytic reactions.

METHODS

As previously described, magnetite production was achieved by the reduction of Fe(III)−oxyhydroxide in the presence of AQDS using *G. sulfurreducens*,[17] under an atmosphere of N_2-CO_2 (80:20). Bottles were incubated in the dark at 30 °C for 2 days after which magnetite had been produced. The resulting magnetite was washed in degassed deionized water and then resuspended in water using its magnetic properties to separate the mineral from the supernatant. An aliquot of a solution of sodium tetrachloropalladate (Na_2PdCl_4, Sigma-Aldrich CAS no. 13820-53-6) was then added so that the final concentration of Pd was 5% by mass of the magnetite. The magnetite suspension was left overnight in a shaking incubator at 150 rpm and 20 °C. The sample was then washed again twice using degassed, distilled deionized water twice before drying under anoxic conditions.

The time-of-flight secondary ion mass spectrometry (TOF-SIMS) analyses were carried out using the IDLE instrument,[38] which was equipped with a C_{60} primary ion gun.[39] Chemical damage by C_{60} primary ions is far less than by any other primary ion species so that depth profiling of organic samples becomes feasible.[40] Analysis of inorganic material is also improved,[41] enabling comprehensive investigation of mixed samples. Only a few atomic layers are sputtered during each measurement, making TOF-SIMS an ideal method to study thin layers on sample surfaces with sensitivities high enough to analyze trace element abundances. As the beam is rastered over the measured area, a complete mass spectrum is recorded at each point, allowing for comprehensive offline analysis. Secondary ion distribution images have been reconstructed for all mass intervals of interest, and background-corrected count integrals for these mass intervals have been used for quantitative analysis. The magnetite samples have been mounted on Al stubs in a thick layer of around 100 μm, and analyses have been carried out with a lateral resolution of 2 μm and a field-of-view of 480 × 365 μm^2.

X-ray absorption (XA) spectra were collected for the Fe and Pd *K*-edges on beamline 9.3 at the Synchrotron Radiation Source (SRS), Daresbury Laboratory. A double crystal Si(311) monochromator was used, detuned to 70% transmission for harmonic rejection. Pd *K*-edges were collected at 80 K in fluorescence mode using a 9-element Ge detector. Fe *K*-edges and a standard palladium foil were collected at 80 K in transmission mode. Background-subtracted EXAFS spectra were analyzed in EXCURV98 using full-curved-wave theory as described in Henderson *et al.*,[42] which allows the proportion of metal in each site to be refined as a single parameter. The metallic phase Pd *K*-edge spectra were analyzed in EXCURV98 using a model based on the crystal structure of Pd[43] and the Fermi energy correction and the absorber−scatterer distances and Debye−Waller factors were refined to minimize a least-squares residual.

XA spectra for XMCD were collected on beamline 4.0.2 at the Advanced Light Source (ALS), Berkeley, CA, using the octopole magnet endstation.[44] Powders were mounted on carbon tape attached to the sample manipulator and kept in O_2-free conditions throughout. XA was monitored in total-electron yield mode, which gives an effective probing depth of ~4.5 nm. At each energy point, the XA was measured for the two opposite magnetization directions by reversing the applied field of 0.6 T. The XA spectra of the two magnetization directions were normalized to the incident beam intensity and subtracted from each other to give the XMCD spectrum.[28] Spectra were fitted by means of a nonlinear least-squares analysis, using calculations for each of the Fe sites.[28] In these calculations, as described elsewhere,[45] the Hartree−Fock−Slater integrals for the 3d−3d and 2p−3d Coulomb and exchange interactions were scaled to 70 and 80%, respectively, and the crystal fields for the O_h and T_d sites were taken to be $10Dq = 1.2$ and -0.6 eV, respectively. The calculated spectra were convoluted by a Lorentzian of $\Gamma = 0.3$ (0.5) eV for the L_3 (L_2) edge to account for intrinsic core−hole lifetime broadening and by a Gaussian of $\sigma = 0.15$ eV to account for instrumental broadening.

TEM was conducted using a Phillips/FEI CM200 equipped with a field emission gun, EDX system (Oxford Instruments UTW ISIS), and a Gatan imaging filter. All TEM images presented here are bright-field images obtained using an operating beam voltage of 200 keV. Selected area electron diffraction (SAED) patterns were acquired using an appropriate diffraction aperture. A droplet of washed sample was placed on a carbon grid (Agar Scientific) and allowed to dry before imaging.

X-ray photoelectron spectroscopy (XPS) data were recorded using a Kratos Axis Ultra employing a monochromated Al Kα X-ray source and an analyzer pass energy of 20 eV, resulting in a total energy resolution of ~0.9 eV. Uniform charge neutralization of the photoemitting surface was achieved by exposing the surface to low-energy electrons in a magnetic immersion lens system (Kratos Ltd.). The system base pressure was 5×10^{-10} mbar. All samples were dried anaerobically, and the resulting powders were loaded into the spectrometer *via* a dry nitrogen glovebox to avoid exposure to atmospheric oxygen. Photoelectron binding energies (BE) were referenced to C1s adventitious carbon contamination peaks set at 285 eV BE. The electron energy analyzer was calibrated using elemental references: Au $4f_{7/2}$ (83.98 eV BE), Ag $3d_{5/2}$ (368.26 eV BE), and Cu $2p_{3/2}$ (932.67 eV BE). An appropriate (Shirley) background was removed from all spectra.[46]

To test the catalytic properties of the Pd-coated biomagnetite dry DMF (15 mL), 5 wt % Pd magnetite catalyst (10.6 mg, 0.5 mol %), iodobenzene (204 mg, 1 mmol), and trienthylamine (0.21 mL, 1.5 mmol) were added to a two-neck round-bottomed flask, equipped with a reflux condenser under a nitrogen atmosphere, and the mixture was heated to 120 °C with stirring. Olefin substrate (1.5 mmol) was added and the mixture stirred at 120 °C under nitrogen. Samples were taken from the reaction periodically for analysis by high-performance liquid chromatography using a Dionex Summit HPLC (with Chromeleon software) with a Summit p580 quaternary low-pressure gradient pump, Summit UVD 170s UV/vis multichannel detector with analytical flow cell, and a Phenomenex Luna 10u C18 (2) column, 250 mm × 4.6 i.d. A flow rate of 1 mL/min was used with a solvent gradient of 100% water to 100% MeCN over 40 min, held for 10 min, and then back to 100% water for 10 min. At the end of the reaction, the mixture was allowed to cool to room temperature before decanting the solution from the flask while retaining the catalyst by applying a magnetic field to the outside of the flask. The solid was washed (5 mL of DMF followed by 5 mL of acetone) and the solid dried for use in the next run.

Acknowledgment. This work was supported by the EPSRC Grants EP/D057310/1 abd EP/D058767/1 and BBSRC Grant BB/E003788/1 and the NERC EnviroSync programme. We would like to thank P. Wincott for XPS analysis, M. Ward for TEM support, and J. Waters for XRD support. We thank the STFC, Daresbury, for beamtime, and S. Fiddy for assistance with EXAFS. The Ad-

vanced Light Source is supported by the Director, Office of Science, Office of Basic Energy Sciences, of the U.S. Department of Energy under Contract No. DE-AC02-05CH11231 and is thanked for XMCD beamtime.

REFERENCES AND NOTES

1. D'Souza, D. M.; Muller, T. J. J. Multi-Component Syntheses of Heterocycles by Transition-Metal Catalysis. *Chem. Soc. Rev.* **2007**, *36*, 1095–1108.
2. Lu, A.-H.; Salabas, E. L.; Schuth, F. Magnetic Nanoparticles: Synthesis, Protection, Functionalization and Application. *Angew. Chem.* **2007**, *46*, 1222–1244.
3. Baruwati, B.; Guin, D.; Manorama, S. V. Pd on Surface-Modified $NiFe_2O_4$ Nanoparticles: A Magnetically Recoverable Catalyst for Suzuki and Heck Reactions. *Org. Lett.* **2007**, *9*, 5377–5380.
4. Guin, D.; Baruwati, B.; Manorama, S. V. Pd on Amine-Terminated Ferrite Nanoparticles: A Complete Magnetically Recoverable Facile Catalyst for Hydrogenation Reactions. *Org. Lett.* **2007**, *9*, 1419–1421.
5. Stevens, P. D.; Fan, J.; Gardimalla, H. M. R.; Yen, M.; Gao, Y. Superparamagnetic Nanoparticle-Supported Catalysis of Suzuki Cross-Coupling Reactions. *Org. Lett.* **2005**, *7*, 2085–2088.
6. Creamer, N. J.; Mikheenko, I. P.; Yong, P.; Deplanche, K.; Sanyahumbi, D.; Wood, J.; Pollmann, K.; Merroun, M.; Selenska-Pobell, S.; Macaskie, L. E. Novel Supported Pd Hydrogenation Bionanocatalyst for Hybrid Homogeneous/Heterogeneous Catalysis. *Catal. Today* **2007**, *128*, 80–87.
7. Wang, Z.; Xiao, P.; Shen, B.; He, N. Synthesis of Palladium-Coated Magnetic Nanoparticle and Its Application in Heck Reaction. *Colloids Surf., A* **2006**, *276*, 116–121.
8. Wang, Z. L.; Shen, B.; Aihua, Z.; He, N. Synthesis of Pd/Fe_3O_4 Nanoparticle-Based Catalyst for the Cross-Coupling of Acrylic Acid with Iodobenzene. *Chem. Eng. J.* **2005**, *113*, 27–34.
9. Rossi, L.; Silva, F. P.; Vono, L. L. R.; Kiyohara, P. K.; Duarte, E. L.; Itri, R.; Landers, R.; Machado, G. Superparamagnetic Nanoparticle-Supported Palladium: A Highly Stable Magnetically Recoverable and Reusable Catalyst for Hydrogenation Reactions. *Green Chem.* **2007**, *9*, 379–385.
10. Mizukoshi, Y.; Sato, K.; Konno, T. J.; Masahashi, N.; Tanabe, S. Magnetically Retrievable Palladium/Maghemite Nanocomposite Catalysts Prepared by Sonochemical Reduction Method. *Chem. Lett.* **2008**, *37*, 922–923.
11. Laska, U.; Frost, C. G.; Price, G. J.; Plucinski, P. K. Easy-Separable Magnetic Nanoparticle-Supported Pd Catalysts: Kinetics, Stability and Catalyst Re-use. *J. Catal.* **2009**, *268*, 318–328.
12. Kinoshita, T.; Seino, S.; Mizukoshi, Y.; Nakagawa, T.; Yamamoto, T. Functionalization of Magnetic Gold/Iron-Oxide Composite Nanoparticles with Oligonucleotides and Magnetic Separation of Specific Target. *J. Magn. Magn. Mater.* **2007**, *311*, 255–258.
13. Mandal, M.; Kundu, S.; Ghosh, S.; Panigrahi, S.; Sau, T.; Yusuf, S.; Pal, T. Magnetite Nanoparticles with a Tunable Gold or Silver Shell. *J. Colloid Interface Sci.* **2005**, *286*, 187–194.
14. Auer, E.; Freund, A.; Pietsch, J.; Tacke, T. Carbons as Supports for Industrial Precious Metal Catalysts. *Appl. Catal., A* **1998**, *173*, 259–271.
15. Lovley, D. R.; Stoltz, J. F.; Nord Jr, G. L.; Phillips, E. J. P. Anaerobic Production of Magnetite by a Dissimilatory Iron-Reducing Microorganism. *Nature* **1987**, *330*, 252–254.
16. Moon, J.-W.; Yeary, L. W.; Rondinone, A. J.; Rawn, C. J.; Kirkham, M. J.; Roh, Y.; Love, L. J.; Phelps, T. J. Magnetic Response of Microbially Synthesized Transition Metal- and Lanthanide-Substituted Nanosized Magnetites. *J. Magn. Magn. Mater.* **2007**, *313*, 283–292.
17. Coker, V. S.; Pearce, C. I.; Pattrick, R. A. D.; van der Laan, G.; Telling, N. D.; Charnock, J. M.; Arenholz, E.; Lloyd, J. R. Probing the Site Occupancies of Co, Ni and Mn Substituted Biogenic Magnetite Using XAS and XMCD. *Am. Mineral.* **2008**, *93*, 1119–1132.
18. Staniland, S.; Williams, W.; Telling, N. D.; van der Laan, G.; Harrison, A.; Ward, B. Controlled Cobalt Doping of Magnetosomes *In Vivo*. *Nat. Nanotechnol.* **2008**, *3*, 158–162.
19. Blakemore, R. Magnetotactic Bacteria. *Science* **1975**, *190*, 377–379.
20. Frankel, R. B.; Blakemore, R.; Wolfe, R. S. Magnetite in Freshwater Magnetic Bacteria. *Science* **1979**, *203*, 1355–1357.
21. Caccavo, F., Jr.; Lonergan, D. J.; Lovley, D. R.; Davis, M.; Stolz, J. F.; McInerney, M. J. *Geobacter sulfurreducens* sp. nov., a Hydrogen and Acetate-Oxidizing Dissimilatory Metal Reducing Bacterium. *Appl. Environ. Microbiol.* **1994**, *60*, 3752–3759.
22. Coker, V. S.; Bell, A. M. T.; Pearce, C. I.; Pattrick, R. A. D.; van der Laan, G.; Lloyd, J. R. Time-Resolved Synchrotron X-ray Powder Diffraction Study of Magnetite Formation by the Fe(III)-Reducing Bacterium *Geobacter sulfurreducens*. *Am. Mineral.* **2008**, *93*, 540–547.
23. Hansel, C. M.; Benner, S. G.; Neiss, J.; Dohnalkova, A.; Kukkadapu, R. K.; Fendorf, S. Secondary Mineralization Pathways Induced by Dissimilatory Iron Reduction of Ferrihydrite under Advective Flow. *Geochim. Cosmochim. Acta* **2003**, *67*, 2977–2992.
24. Beletskaya, I. P.; Cheprakov, A. V. The Heck Reaction as a Sharpening Stone of Palladium Catalysis. *Chem. Rev.* **2000**, *100*, 3009–3066.
25. Polshettiwar, V.; Molnár, Á. Silica-Supported Pd Catalysts for Heck Coupling Reactions. *Tetrahedron* **2007**, *63*, 6949–6976.
26. Wang, Z.; Chen, Z.; Gu, J.; Li, Y.; Li, W. Occurrence and Environmental Implications of Magnetic Iron Sulfides in Stiff Muds from the Continental Shelf of the East China Sea. *Geo-Mar. Lett.* **2005**, *25*, 300–305.
27. Marshall, M. J.; Beliaev, A. S.; Dohnalkova, A. C.; Kennedy, D. W.; Shi, L.; Wang, Z.; Boyanov, M. I.; Lai, B.; Kemner, K. M.; McLean, J. S. c-Type Cytochrome-Dependent Formation of U(IV) Nanoparticles by *Shewanella oneidensis*. *PLoS Biol.* **2006**, *4*, e268.
28. Pattrick, R. A. D.; van der Laan, G.; Henderson, C. M. B.; Kuiper, P.; Dudzik, E.; Vaughan, D. J. Cation Site Occupancy in Spinel Ferrites Studied by X-ray Magnetic Circular Dichroism: Developing a Method for Mineralogists. *Eur. J. Mineral.* **2002**, *14*, 1095–1102.
29. Pearce, C. I.; Henderson, C. M. B.; Pattrick, R. A. D.; van der Laan, G.; Vaughan, D. J. Direct Determination of Cation Site Occupancies in Natural Ferrite Spinels by $L_{2,3}$ X-ray Absorption Spectroscopy and X-ray Magnetic Circular Dichroism. *Am. Mineral.* **2006**, *91*, 880–893.
30. Coker, V. S.; Gault, A. G.; Pearce, C. I.; van der Laan, G.; Telling, N. D.; Charnock, J. M.; Polya, D. A.; Lloyd, J. R. XAS and XMCD Evidence for Species-Dependent Partitioning of Arsenic during Microbial Reduction of Ferrihydrite to Magnetite. *Environ. Sci. Technol.* **2006**, *40*, 7745–7750.
31. Carvallo, C.; Sainctavit, P.; Arrio, M.-A.; Menguy, N.; Wang, Y.; Ona-Nguema, G.; Brice-Profeta, S. Biogenic *vs.* Abiogenic Magnetite Nanoparticles: A XMCD Study. *Am. Mineral.* **2008**, *93*, 880–885.
32. Coker, V. S.; Pearce, C. I.; Lang, C.; van der Laan, G.; Pattrick, R. A. D.; Telling, N. D.; Schuler, D.; Arenholz, E.; Lloyd, J. R. Cation Site Occupancy of Biogenic Magnetite Compared to Polygenic Ferrite Spinels Determined by X-ray Magnetic Circular Dichroism. *Eur. J. Mineral.* **2007**, *19*, 707–716.
33. Wagner, C. D.; Riggs, W. M.; Davis, L. E.; Moulder, J. F.; Muilenberg, G. E., *Handbook of X-ray Photoelectron Spectroscopy*; Perkin Elmer Corporation: Eden Prairie, MN, 1979.
34. Kim, K. S.; Gossmann, A. F.; Winograd, N. X-ray Photoelectron Spectroscopic Studies of Palladium Oxides and the Palladium-Oxygen Electrode. *Anal. Chem.* **1974**, *46*, 197–200.
35. Bonnemann, H.; Brinkmann, R.; Neiteler, P. Preparation and Catalytic Properties of NR^+_4-Stabilized Palladium Colloids. *Appl. Organomet. Chem.* **1994**, *8*, 361–378.
36. Reetz, M. T.; Breinbauer, R.; Wanninger, K. Suzuki and Heck Reactions Catalyzed by Preformed Palladium Clusters and

Palladium/Nickel Bimetallic Clusters. *Tetrahedron Lett.* **1996**, *37*, 4499–4502.
37. Reetz, M. T.; Helbig, W.; Quaiser, S. A.; Stimming, U.; Breuer, N.; Vogel, R. Visualization of Surfactants on Nanostructured Palladium Clusters by a Combination of STM and High-Resolution TEM. *Science* **1995**, *267*, 367–369.
38. Henkel, T.; Tizard, J.; Blagburn, D.; Lyon, I. IDLE—Interstellar Dust Laser Explorer. A New Instrument for Elemental and Isotopic Analysis and Imaging of Interstellar and Interplanetary Dust. *Rev. Sci. Instrum.* **2007**, *78*, 055107.
39. Hill, R.; Blenkinsopp, P. W. M. The Development of C_{60} and Gold Cluster Ion Guns for Static SIMS Analysis. *Appl. Surf. Sci.* **2004**, *231−232*, 936–939.
40. Fletcher, J. S.; Conlan, X. A.; Jones, E. A.; Biddulph, G.; Lockyer, N. P.; Vickerman, J. C. TOF-SIMS Analysis Using C_{60}. Effect of Impact Energy on Yield and Damage. *Anal. Chem.* **2006**, *78*, 1827–1831.
41. Henkel, T.; Rost, D.; Lyon, I. C. Improvements in Quantification Accuracy of Inorganic Time-of-Flight Secondary Ion Mass Spectrometric Analysis of Silicate Materials by Using C_{60} Primary Ions. *Rapid Commun. Mass Spectrom.* **2009**, *23*, 3355–3360.
42. Henderson, C. M. B.; Charnock, J. M.; Plant, D. A. Cation Occupancies in Mg, Co, Ni, Zn, Al Ferrite Spinels: A Multi-Element Approach EXAFS Study. *J. Phys.: Condens. Matter* **2007**, *19*, 076214.
43. Rao, C. N.; Rao, K. K. Effect of Temperature on Lattice Parameters of Some Silver-Palladium Alloys. *Can. J. Phys.* **1964**, *42*, 1336–1342.
44. Arenholz, E.; Prestemon, S. O. Design and Performance of an Eight-Pole Resistive Magnet for Soft X-ray Magnetic Dichroism Measurements. *Rev. Sci. Instrum.* **2005**, *76*, 083908/1–083908/8.
45. van der Laan, G.; Thole, B. T. Strong Magnetic X-ray Dichroism in 2p Absorption Spectra of 3d Transition Metal Ions. *Phys. Rev. B* **1991**, *43*, 13401–13411.
46. Shirley, D. A. High-Resolution X-ray Photoemission Spectrum of the Valence Bands of Gold. *Phys. Rev. B* **1972**, *5*, 4709–4714.